RSC Advances

PAPER

Cite this: *RSC Adv.*, 2018, **8**, 19213

Enhanced efficiency of $Cu_2ZnSn(S,Se)_4$ solar cells *via* anti-reflectance properties and surface passivation by atomic layer deposited aluminum oxide

Bingye Zhang, *[a] Lu Han,[a] Shitian Ying,[a] Yongfeng Li[b] and Bin Yao*[b]

Reducing interface recombination losses is one of the major challenges in developing $Cu_2ZnSn(S,Se)_4$ (CZTSSe) solar cells. Here, we propose a CZTSSe solar cell with an atomic layer deposited Al_2O_3 thin film for surface passivation. The influence of passivation layer thickness on the power conversion efficiency (PCE), short-circuit current density (J_{sc}), open-circuit voltage (V_{oc}) and fill factor (FF) of the solar cell is systematically investigated. It is found that the Al_2O_3 film presents notable antireflection (AR) properties over a broad range of wavelengths (350–1000 nm) for CZTSSe solar cells. With increasing Al_2O_3 thickness (1–10 nm), the average reflectance of the CZTSSe film decreases from 12.9% to 9.6%, compared with the average reflectance of 13.6% for the CZTSSe film without Al_2O_3. The Al_2O_3 passivation layer also contributes to suppressed surface recombination and enhanced carrier separation. Passivation performance is related to chemical and field effect passivation, which is due to released H atoms from the Al–OH bonds and the formation of Al vacancies and O interstitials within Al_2O_3 films. Therefore, the J_{sc} and V_{oc} of the CZTSSe solar cell with 2 nm-Al_2O_3 were increased by 37.8% and 57.8%, respectively, in comparison with those of the unpassivated sample. An optimal CZTSSe solar cell was obtained with a V_{oc}, J_{sc} and η of 0.361 V, 33.78 mA and 5.66%. Our results indicate that Al_2O_3 films show the dual functions of AR and surface passivation for photovoltaic applications.

Received 21st April 2018
Accepted 15th May 2018

DOI: 10.1039/c8ra03437k

rsc.li/rsc-advances

1. Introduction

Recently, it has been proven that the conversion efficiencies of $Cu(In,Ga)Se_2$ (CIGS) thin film solar cells can reach 22.6%, which is comparable to their Si counterparts.[1,2] However, the shortage and high material cost of indium and gallium restrict the development of CIGS solar cells. Kesterite $Cu_2ZnSn(S,Se)_4$ (CZTSSe) has attracted much more attention as a promising substitute for CIGS solar cells on account of its outstanding optoelectronic properties and earth abundant, as well as non-toxic, constituents.[3,4] The kesterite structure of CZTSSe is derived from the chalcopyrite crystal structure of CIGS, where Zn^{2+} and Sn^{4+} ions replace an equal number of In^{3+} and Ga^{3+} ions.[5,6] Since it has similar properties to CIGS solar cells, the structure of a CZTSSe solar cell is adopted directly from CIGS photovoltaic technology, including a Mo bottom electrode, a chemical bath deposited CdS buffer layer, a transparent conducting oxide (TCO) stack of indium tin oxide (ITO)/ZnO *etc.* Recently, the conversion efficiency record of CZTSSe solar cells has been proven to be 12.6% using a hydrazine solution based method.[7] However, the efficiency of CZTSSe solar cells remains far from that of CIGS solar cells. To decrease the efficiency gap between CZTSSe and CIGS solar cells, one of the major challenges is reducing surface carrier recombination, which is caused by grain boundaries, defects and states. Various technologies have been utilized to fabricate high quality CZTSSe films, such as thermal coevaporation, sputtering, pulsed-laser deposition and other non-vacuum-deposition technologies (*e.g.* electrodeposition and solution processing).[8–11] However, due to the complexity of multernary materials, it is difficult to obtain high quality CZTSSe films with a low density of defects and states at the interface between CZTSSe and CdS. Thus, CZTSSe devices suffer from an open-circuit voltage (V_{oc}) deficit caused by the significant recombination of photo-excited carriers due to the existence of large amounts of defects/states at the interface between CZTSSe and CdS.[12,13] To solve this problem, it is necessary to induce a passivation layer to depress recombination. On one hand, a proper passivation layer can not only saturate dangling bonds to decrease the density of surface states in CZTSSe films (called chemical passivation), but also reduce the surface recombination velocity (S_{eff}) due to the existence of fixed charge in the passivation layer (called field effect passivation).[14,15] On the other hand, passivation layers can

[a]*Department of Physics, Dalian University of Technology, Dalian, Liaoning, 116023, P. R. China. E-mail: byzhang@dlut.edu.cn*

[b]*Key Laboratory of Physics and Technology for Advanced Batteries (Ministry of Education), College of Physics, Jilin University, Changchun 130012, China. E-mail: binyao@jlu.edu.cn*

also prevent atomic interdiffusion between different layers in PV devices.[16,17] Several dielectric materials have been used as passivation layers in CZTS-based solar cells and other PV devices (CIGS, Si solar cells *etc.*), such as Al_2O_3, TiO_2, Si_3N_4 and ZrO_2.[18–22] Among these materials, Al_2O_3 has been regarded as a favorable material owing to its high dielectric constant, high transmission and large bandgap (6.3 eV), and is able to passivate p- and n-type semiconductors effectively.[23,24] Recently, atomic layer deposition (ALD) has been proven to be an optimal technique for the synthesis of virtually pinhole-free inorganic thin films due to its low temperature deposition and precise thickness control. Moreover, atomic layer deposited Al_2O_3 (ALD-Al_2O_3) can provide a state-of-the-art level of surface passivation on c-Si ($S_{eff} < 2$ cm s^{-1}) and CIGS solar cells ($S_{eff} < 14$ cm s^{-1}).[25,26] These low S_{eff} values for Al_2O_3 passivated Si and CIGS solar cells are attributed to the high density negative fixed charge ($Q_f = 10^{12}$–10^{13} cm^{-2}) in Al_2O_3 and the low interface-trap charge density ($D_{it} = 10^{10}$–10^{12} eV^{-1} cm^{-2}) at the interfaces of Al_2O_3/Si and Al_2O_3/CIGS. These positive results for the Al_2O_3 passivation layer and the beneficial technical aspects of ALD itself suggest that they would be appropriate for the passivation of CZTSSe solar cells.

As is well known, the thickness of Al_2O_3 plays an important role in the density of interface states and the negative fixed charge for Si solar cells.[27] Therefore, identifying the optimal thickness of Al_2O_3 thin film has become the critical factor for obtaining high passivation performance for CZTSSe solar cells. However, few reports describe the influence of Al_2O_3 thickness on the device performance of CZTSSe solar cells. Moreover, due to the differences in the structural, electronic and defect properties of CZTSSe and Si, as well as CIGS, the dominant passivation mechanism of Al_2O_3 on CZTSSe is still unclear.

In this study, CZTSSe films (Cu/(Zn + Sn) = 0.81 and S/(S + Se) = 0.12) coated with various thicknesses of ALD-Al_2O_3 (1–10 nm) film were fabricated. The influence of Al_2O_3 thickness on the optical and electrical properties of CZTSSe solar cells was investigated in detail. We demonstrate that ALD-Al_2O_3 thin films can not only provide a passivation effect, but also show excellent antireflection (AR) properties at short wavelengths for CZTSSe solar cells, which improves the power conversion efficiency (PCE), V_{oc}, FF and short-circuit current density (J_{sc}) of the CZTSSe solar cells. A CZTSSe solar cell with a PCE of 5.66% has been achieved *via* adjusting the thickness of the Al_2O_3 thin film.

2. Experimental section

2.1. Materials and syntheses

Preparation of CZTS precursor solution. The CZTS precursor solution was prepared by dissolving $Cu(CH_3COO)_2 \cdot H_2O$ (1.198 g, 6 mmol), $SnCl_2 \cdot 2H_2O$ (0.745 g, 3.30 mmol), $ZnCl_2$ (0.5043 g, 3.70 mmol) and thiourea (1.97 g, 26 mmol) into *N*,*N*-dimethylformamide (10 mL, DMF) and then magnetically stirring for 2 h at room temperature. A CZTS thin film with a thickness of ~1.1 μm was fabricated by spin-coating the CZTS precursor solution on molybdenum (Mo)-coated soda lime glass (SLG) substrates at a rotation rate of 3000 rpm for 30 s followed by drying in air at 300 °C for 3 min. The coating and drying processes were repeated 10 times.

Synthesis of CZTSSe absorbers. To obtain CZTSSe films, CZTS precursor films were sealed in a graphite box (~55 mm in diameter and ~40 mL in volume) with 200 mg of selenium. The selenization process was carried out in a rapid thermal processing (RTP) furnace (MTI, OTF-1200X-4-RTP), under nitrogen flow (80 mL min^{-1}) at 550 °C for 15 min with a ramping rate of 300 °C min^{-1}, and finally cooled down to room temperature naturally.

Deposition of Al_2O_3 thin films. Al_2O_3 thin films with varying thickness (1–10 nm) were deposited on CZTSSe by ALD, using trimethylaluminum (TMA), H_2O and high-purity N_2 as Al and O sources, and carrying gas, respectively. The surface chemistry during Al_2O_3 deposition can be described as follows:

$$AlOH^* + Al(CH_3)_3 \rightarrow AlO - Al(CH_3)_2^* + CH_4 \quad (1)$$

$$AlCH_3^* + H_2O \rightarrow Al - OH^* + CH_4 \quad (2)$$

The ALD-Al_2O_3 thin films were fabricated at 220 °C, and then annealed *in situ* at 400 °C for 10 min in N_2 to activate surface passivation. Various thicknesses of the Al_2O_3 thin films were obtained *via* controlling the deposition cycles, and the growth rate of Al_2O_3 was 0.7 Å per cycle. Each cycle consisted of a TMA pulse (0.03 s), an N_2 purge (12 s), a water pulse (0.06 s) and an N_2 purge (12 s).

Fabrication of CZTSSe photovoltaic devices. CZTSSe solar cells were fabricated with the structure SLG/Mo/CZTSSe/Al_2O_3/CdS/i-ZnO/indium tin oxide (ITO)/Al grid. 50 nm thick CdS buffer layers were deposited on the ALD-Al_2O_3 thin films using chemical bath deposition (CBD), and then 50 nm i-ZnO and 250 nm ITO layers were deposited using RF and DC magnetron sputtering sequentially. Finally, top contact fingers were formed with an Al grid electrode (~2 μm) on the ITO layer. All of the solar devices had an active area of 0.20 cm^2, defined by mechanical scribing (~92% of the total device area, 0.22 cm^2).

2.2. Characterization

The structure, surface morphology and compositional ratio of CZTSSe films were measured using scanning electron microscope (SEM) measurements on a Hitachi S-4800 equipped with an energy-dispersive X-ray spectroscopy (EDS) system (EDAX Genesis 2000). The crystal structures of the CZTSSe films were characterized using an X-ray diffractometer (XRD) with Cu Kα radiation ($\lambda = 1.5406$ Å). Optical reflectance of the CZTSSe films with ALD-Al_2O_3 thin films was detected using a spectrophotometer with an integrating sphere. X-ray photoelectron spectroscopy (XPS) analysis was used to identify the actual composition and chemical state of the grown Al_2O_3 thin films. For the PCE measurements of the CZTSSe solar cells, current density–voltage curves were measured using a Keithley 2400 source meter and a solar simulator (Abet Sun 2000; AM 1.5). The light intensity was calibrated to 100 mW cm^{-2} using a Newport optical power meter (model 842-PE) certified by Newport. The external quantum efficiency (EQE) curves were measured using

a Zolix SCS100 QE system equipped with a 150 W xenon light source, a lock-in amplifier and an integrating sphere.

3. Results and discussion

In general, most passivation materials need a post deposition annealing (PDA) process to activate the passivation effect.[17] In some cases, the annealing treatment can cause the deterioration of crystalline quality for the films deposited under low temperatures, leading to more defects and impurities. Thus, SEM and XRD measurements were carried out to specify whether PDA could cause degradation. Fig. 1 shows top-view and cross-sectional SEM images for the CZTSSe films and the devices. Both of the CZTSSe films, with and without the Al_2O_3 thin film, exhibit a compact and dense morphology with a grain size ranging from 1–2 μm, as shown in Fig. 1(a) and (b). Fig. 1(c) and (d) show cross-sectional SEM images of the CZTSSe solar cell, which consists of a 1 μm Mo film, a 1.17 μm CZTSSe film, a 2 nm Al_2O_3 thin film, and a 50 nm CdS film, as well as a 300 nm i-ZnO/ITO film. It can be seen that the compactness and domain size of CZTSSe coated with Al_2O_3 thin film aren't obviously changed compared with the unpassivated sample, which demonstrates that the deposition and annealing processes of Al_2O_3 have a faint effect on the surface morphology and the grain growth of CZTSSe films. It should be noted that some holes exist at the interface between CZTSSe and Mo, which is assigned to the unstable nature of CZTSSe in contact with Mo.[28]

Fig. 2 shows the XRD patterns of CZTSSe films, with and without Al_2O_3 thin film. The XRD patterns of the CZTSSe films show that all of the films can be indexed in kesterite-type structures with no secondary phases.[29] With reference to JCPDS no. 00-026-0575 and 00-052-0868, three major diffraction peaks located at 27.34°, 45.45° and 53.81° are observed, which can be assigned to the (112), (220) and (312) planes, respectively, implying the good crystallinity of CZTSSe films. In addition, a minor peak located at 36.40° is also observed, corresponding to the (211) diffraction plane, as shown in Fig. 2(a). Fig. 2(b) shows the XRD pattern of the CZTSSe film with 2 nm Al_2O_3 thin film. Besides the diffraction peaks of CZTSSe, it can be clearly seen that no diffraction peak belonging to Al_2O_3 can be observed, suggesting the amorphous phase of the ALD-Al_2O_3 thin film. Moreover, the XRD peak position and full width at half-maximum (FWHM) of CZTSSe shows little change after the

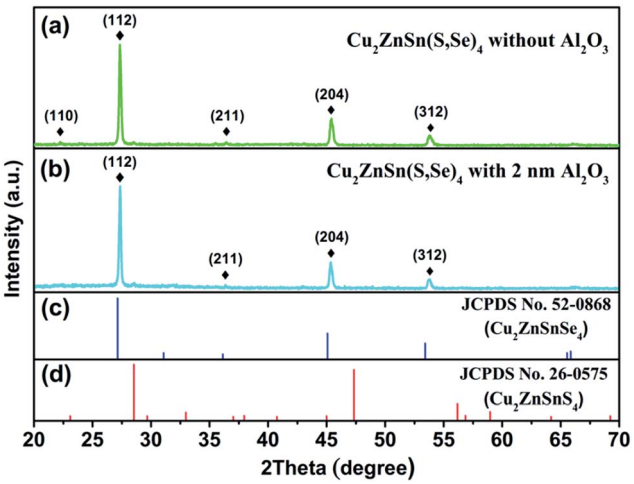

Fig. 2 XRD patterns of CZTSSe films (a) without Al_2O_3 thin film and (b) with 2 nm Al_2O_3 thin film, as well as the standard patterns for (c) CZTSe (JCPDS no. 82-0868) and (d) CZTS (JCPDS no. 26-0575).

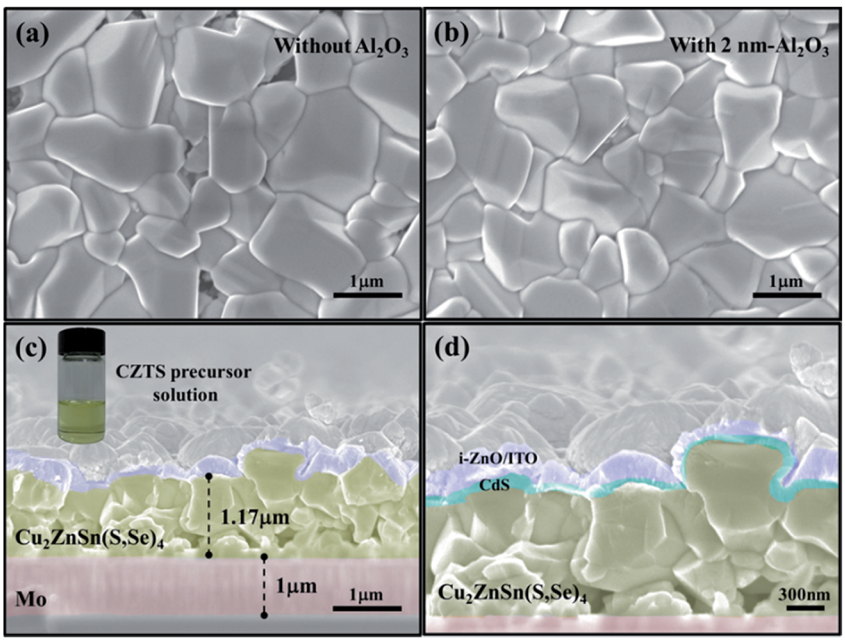

Fig. 1 Top-views of the CZTSSe film with and without Al_2O_3 thin film (a and b), deposited on a Mo-coated SLG substrate. Cross-sectional SEM images of the CZTSSe solar cell with the structure SLG/Mo/CZTSSe/Al_2O_3 (2 nm)/CdS/i-ZnO/ITO/Al grid (c and d).

Al_2O_3 deposition and PDA processes. These results indicate that the processes of Al_2O_3 deposition and PDA have no obvious influence on the crystalline quality of CZTSSe film, which is consistent with the SEM results.

For quantitative phase analysis, the full profile Rietveld refinement of the XRD pattern of the CZTSSe powder was carried out, as shown in Fig. 3. The structural model was refined on the basis of the tetragonal kesterite-type crystal structure [space group: $I\bar{4}$ (no. 82)]. The obtained structural parameters of CZTSSe are $a = 5.6573$ Å, $c = 11.301$ Å, and $c/a = 2.00$. The corresponding weighted residual error (R_{wp}), residual of least-squares refinement (R_p) and χ^2 of the fittings are 5.87%, 4.46%, and 2.38, indicating good fits of the patterns. These lattice parameters (a and c) are slightly decreased compared to the reported values of CZTSe (ICSD#95117). This decreasing of the lattice parameters can be assigned to the shrinkage of the unit cell due to the substitution of Se atoms with S, which have a smaller ionic radius (1.84 Å) compared to that of Se (1.98 Å).[30]

Reducing optical losses is an important way to increase the density of photo-generated carriers for PV devices. Therefore, an AR layer is usually adopted to realize the low reflectance of solar cells, such as MgF_2, SiO_2 and SiN_x:H in CIGS and Si PV devices.[31,32] Several reports have proven that Al_2O_3 can have good AR properties with wide thickness ranges for Si solar cells.[33] To verify the AR performance of Al_2O_3 in CZTSSe solar cells, the reflectance spectra of CZTSSe with various thicknesses of Al_2O_3 thin films were obtained for wavelengths from 350 nm to 1250 nm, as shown in Fig. 4(a). A remarkable decrease in the total reflectance of CZTSSe with Al_2O_3 thin films can be observed over a wide spectral range. The spectrum-weighted average reflectance (R_{ave}) can be defined as:[34]

$$R_{ave} = \frac{\int_{350}^{1250} R(\lambda)N(\lambda)\mathrm{d}\lambda}{\int_{350}^{1250} N(\lambda)\mathrm{d}\lambda} \quad (3)$$

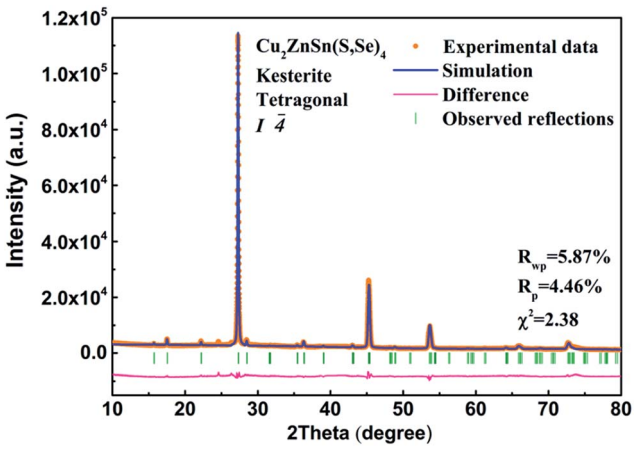

Fig. 3 Rietveld refined X-ray diffraction profile of CZTSSe film, where the orange dots are experimental data, the blue line is the obtained fit, the green ticks are the Bragg peak positions of the kesterite-type structure, and the pink line is the difference between the experimental and calculated data.

where $R(\lambda)$ is the total reflectance and $N(\lambda)$ is the solar flux under the standard conditions of AM 1.5. By calculation, the R_{ave} values of the as-deposited CZTSSe and CZTSSe with 1 nm, 2 nm, 5 nm and 10 nm Al_2O_3 thin films are 13.6%, 12.9%, 12.1%, 10.9% and 9.6%, respectively. With increasing Al_2O_3 thickness, the R_{ave} value of CZTSSe decreases by 32.4%, implying the good AR performance of Al_2O_3 thin film. The inset in Fig. 4(a) shows the CZTSSe solar cell with and without Al_2O_3 thin film, which shows a significant reduction in reflection losses for the CZTSSe solar cells. Fig. 4(b) shows the R_{ave} of CZTSSe/Al_2O_3 as a function of Al_2O_3 thickness and the ALD deposition cycles, and the inset shows digital photographs of CZTSSe film with various thicknesses of Al_2O_3 thin films. The R_{ave} exhibits an exponential reduction with increasing Al_2O_3 thickness, as shown in Fig. 4(b). For the bare CZTSSe film, a high R_{ave} of 13.6% is observed. After depositing 1 nm Al_2O_3 thin film, the R_{ave} of CZTSSe/Al_2O_3 decreases about 0.7%. With increasing Al_2O_3 thickness, the R_{ave} of CZTSSe/Al_2O_3 decreases continuously, reaching 9.6% at the Al_2O_3 thickness of 10 nm. We have noticed that the reflectance of CZTSSe/Al_2O_3 decreases faster at short wavelengths (350–650 nm) than at long wavelengths (650–1100 nm) with increasing Al_2O_3 thickness. The reflectance of CZTSSe with 10 nm Al_2O_3 decreases beyond 60% at short wavelengths compared with 13% at long wavelengths. The discrepancy in reflectance at different wavelengths is mainly due to the dispersion of the Al_2O_3 refractive index.[33] These results imply that the Al_2O_3 thin film can provide satisfying AR performance, especially in short wavelength regions, which can increase photo-generated carriers effectively.

Besides its AR properties, Al_2O_3 thin film can also provide an excellent passivation effect for both p- and n-type materials. In order to explore the origin of the passivation mechanism of Al_2O_3 on CZTSSe, the chemical states of Al and O were identified through XPS measurements. Fig. 5 shows the XPS spectra of Zn 2p, Al 2p and O 1s, respectively. The Zn 2p spectrum consists of two narrow peaks at 1022.5 eV and 1045.5 eV, corresponding to Zn $2p_{1/2}$ and $2p_{3/2}$, with a peak splitting of $\Delta E = 23.0$ eV, in accordance with the standard splitting of 23 eV for Zn(II) state, as shown in Fig. 5(a).[35] The O 1s core-level XPS spectra of Al_2O_3 thin film is shown in Fig. 5(b). The O 1s spectrum can be fitted into two peaks, located at 531.4 eV and 532.6 eV, which are attributed to Al–O–Al bonds and Al–OH bonds.[33] The appearance of hydroxyl groups can be assigned to an incomplete reaction during eqn (1) and adsorbed H_2O on the surface.[36] Fig. 5(c) shows the Al 2p core-level XPS spectra of the as-deposited and annealed Al_2O_3 thin film. For the as-deposited sample, the Al 2p peak with a binding energy of 75.2 eV is assigned to the Al–O bond, which can be fitted into two sub-spectra located at 74.2 eV and 75.6 eV, corresponding to O–Al–O bonds and Al–OH bonds, respectively.[35] After annealing, the component at 75.6 eV disappears, while the peak with a binding energy of 74.2 eV remains, indicating the disappearance of Al–OH bonds during the annealing process. According to previous literature, the residual O–H bonds would be broken easily to release interstitial O and interstitial H atoms during the annealing process.[37] The interstitial H ions migrate through the Al_2O_3 matrix and arrive at the Al_2O_3/CZTSSe interface to

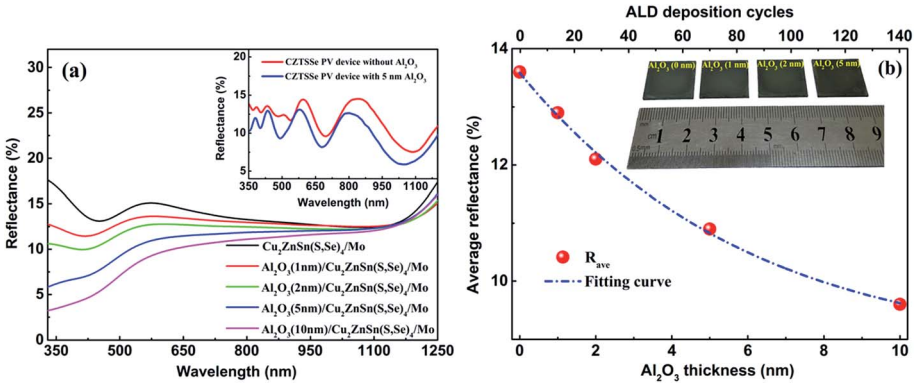

Fig. 4 (a) The reflectance spectra of CZTSSe thin films without Al_2O_3 thin film and with Al_2O_3 thin film at various thicknesses. The inset is the reflectance spectra of CZTSSe solar cells without Al_2O_3 thin film and with 5 nm Al_2O_3 thin film. (b) The R_{ave} of CZTSSe thin films coated with Al_2O_3 thin films as a function of Al_2O_3 thickness and ALD cycles. The inset is digital photographs of CZTSSe thin films with Al_2O_3 thin film at various thicknesses.

passivate the dangling bonds or grain boundaries of the CZTSSe film.[38] Meanwhile, the excess O ions released from hydroxyl groups are also helpful for the formation of O interstitials (O_i), which are responsible for the negative fixed charge in Al_2O_3 thin film, leading to the enhancement of field-effect passivation.[37] Furthermore, negative fixed charge at the interface between CZTSSe and Al_2O_3 can effectively strengthen the built-in field of the p–n junction, which can enhance the carrier-separation efficiency.

To further understand the effects of passivation on device performance, the photovoltaic investigation of CZTSSe solar cells with the structure SLG/Mo/CZTSSe/Al_2O_3/CdS/i-ZnO/ITO/Al was carried out. Fig. 6 displays current density–voltage (J–V) curves for CZTSSe solar cells with various thicknesses of Al_2O_3 under standard AM 1.5 illumination (100 mW cm^{-2}). The detailed device parameters are listed in Table 1. It was found that the unpassivated CZTSSe solar cell achieved a PCE of 2.24%, and the V_{oc}, J_{sc} and FF values are 0.262 V, 21.42 mA cm^{-2} and 38.22%, respectively. After Al_2O_3 deposition, the PCE increased sharply and then decreased with increasing Al_2O_3 thickness from 1 nm to 5 nm. The PCE reached the highest value of 5.66% at a film thickness of 2 nm. The V_{oc}, J_{sc} and FF change similarly to the PCE, revealing the highest values of 0.361 V, 33.78 mA cm^{-2} and 48.98%, respectively. Compared with CZTSSe solar cells without Al_2O_3 passivation, the V_{oc}, J_{sc} and FF values of the CZTSSe with 2 nm Al_2O_3 thin film were increased by 37.8%, 57.8% and 28.2%, respectively. This improvement in device performance can be assigned to the AR

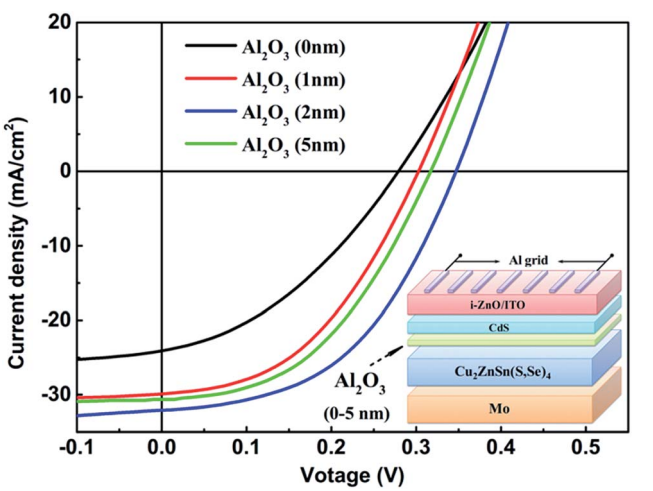

Fig. 6 Current–voltage curves for CZTSSe solar cells with Al_2O_3 thin film at various thicknesses, in comparison with unpassivated CZTSSe solar cells. The inset is the schematic of the device structure.

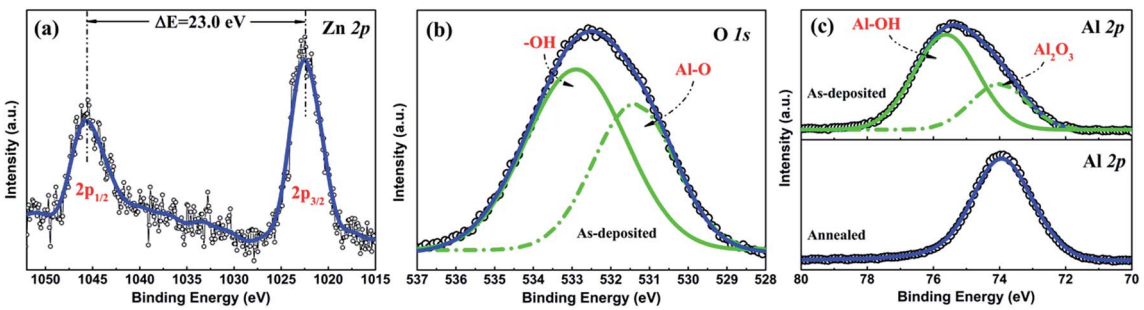

Fig. 5 XPS spectra of (a) the Zn 2p core level of the CZTSSe film, (b) the O 1s core level of as-deposited Al_2O_3, and (c) the Al 2p core-level of as-deposited and annealed Al_2O_3.

Table 1 Detailed device parameters of CZTSSe solar cells with Al_2O_3 thin film at different thicknesses

Al_2O_3 thickness (nm)	V_{oc} (V)	J_{sc} (mA cm^{-2})	FF (%)	Eff. (%)
0	0.262	21.42	38.22	2.24
1	0.301	26.84	39.45	3.12
2	0.361	33.78	48.98	5.66
5	0.312	30.68	46.14	4.39
10	—	—	—	—

performance of Al_2O_3 thin film and the reduction of the density of acceptor-like states at the interface between CZTSSe/Al_2O_3, resulting in the decreased compensation of photo-generated carriers.[13]

Fig. 7(a) displays the EQE spectra of CZTSSe solar cells with various thicknesses of Al_2O_3 passivation layers. For comparison, a CZTSSe solar cell without an Al_2O_3 passivation layer is also added as a reference. All of the CZTSSe solar cells present a distinct spectral response, and with increasing Al_2O_3 thickness, the EQE value shows a similar trend to that of the PCE results. The CZTSSe solar cell with 2 nm Al_2O_3 exhibits the highest value of around 80% in the wavelength region of 500 nm to 900 nm. It is found that the EQE is improved at all wavelengths with increasing Al_2O_3 thickness, especially in the long wavelength region. The improvement in EQE indicates the improvement in the collection length of photo-generated carriers, which is due to the passivation of the CZTSSe surface and/or grain boundaries by Al_2O_3 films.[24] In addition, the bandgap of the CZTSSe films is determined by plotting $[E \times \ln(1 - \mathrm{EQE})]^2$ *versus* E using the EQE spectra of the CZTSSe solar cell, as shown in Fig. 7(b). It is found that the bandgaps of all of the CZTSSe films have the value of 1.07 eV, which indicates that the ALD process has no influence on the stoichiometric ratio of the CZTSSe film, especially the S/Se ratio, which is consistent with the XPS and EDS results. Therefore, it is deduced that the improvement of the performance of CZTSSe solar cells mainly originates from decreases in the reflectance of CZTSSe and the surface passivation of Al_2O_3.

Based on the above discussions, it can be concluded that the development of CZTSSe solar cells originates from two aspects. On one hand, the deposition of Al_2O_3 thin films can reduce the reflectance of CZTSSe films and increase photo-generated carriers, leading to an improvement in device performance, especially the J_{sc} value. On the other hand, Al_2O_3 thin films can not only saturate the defects and dangling bonds at the interface between CZTSSe and CdS, but also produce a large amount of negative fixed charge to reduce interface recombination and increase the carrier separation efficiency, resulting in an increased V_{oc} value. In addition, although thicker Al_2O_3 thin films are beneficial for obtaining lower reflectance for the CZTSSe films, the optimal CZTSSe PV device was obtained at the Al_2O_3 thickness of 2 nm in the present work, which can be explained as follows. According to our results and other literature on Si and CIGS solar cells, a thicker passivation layer causes reduction in the fixed charge, leading to the debasing of field-effect passivation. Therefore, the Al_2O_3 passivation layer should be kept thin enough so that the photo-excited electrons are able to effectively tunnel through the layer in the device.

4. Conclusions

In summary, Al_2O_3 thin films of various thicknesses were deposited on the top of CZTSSe prior to CdS deposition by ALD. The influence of the thickness of Al_2O_3 thin films on the reflectance and PCE values of CZTSSe solar cells was investigated in detail. The CZTSSe without the Al_2O_3 thin film achieved an R_{ave} of 13.6%. After deposition of the Al_2O_3 thin films, the R_{ave} values of CZTSSe films with 1 nm, 2 nm, 5 nm and 10 nm Al_2O_3 were 12.9%, 12.1%, 10.9% and 9.6%, respectively. This decrease in R_{ave} demonstrates that Al_2O_3 thin films can provide favorable AR properties. The XPS results indicate the existence of a large amount of O_i, which is believed to be the origin of field effect passivation caused by the negative fixed charge. The appearance of O_i can not only provide field effect passivation to depress surface recombination, but also enhance the built-in field of the p–n junction to increase the carrier-separation efficiency. The V_{oc}, J_{sc}, and η of CZTSSe solar cells with 2 nm Al_2O_3 thin film achieved the highest values of 0.361 V, 33.78 mA and 5.66%, respectively, in comparison with 0.262 V, 21.42 mA and 2.24% for the CZTSSe solar cell without passivation.

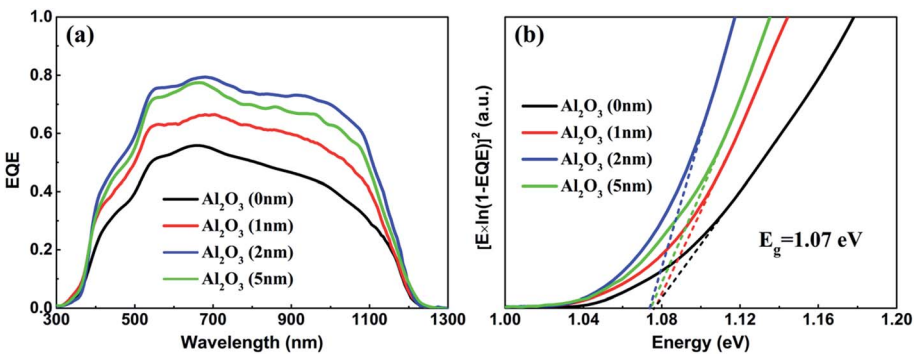

Fig. 7 (a) EQE spectra of CZTSSe solar cells with Al_2O_3 thin film at various thicknesses. (b) Band gap values of CZTSSe solar cells, with Al_2O_3 thin film at various thicknesses, determined by the $[E \times \ln(1 - \mathrm{EQE})]^2$ *vs.* E curve.

Conflicts of interest

There are no conflicts to declare.

Acknowledgements

This work was financially supported by the National Natural Science Foundation of China (Grant No. 61604029 and 61774075) and the Fundamental Research Funds for the Central Universities (Grant No. DUT18LK48).

References

1 P. Jackson, D. Hariskos, R. Wuerz, O. Kiowski, A. Bauer, T. M. Friedlmeier and M. Powalla, *Phys. Status Solidi RRL*, 2015, **9**, 28–31.
2 P. Jackson, R. Wuerz, D. Hariskos, E. Lotter, W. Witte and M. Powalla, *Phys. Status Solidi RRL*, 2016, **10**, 583–586.
3 N. Shibayama, Y. W. Zhang, T. Satake and M. Sugiyama, *RSC Adv.*, 2017, **7**, 25347–25352.
4 Z. Y. Xiao, B. Yao, Y. F. Li, Z. H. Ding, Z. M. Gao, H. F. Zhao, L. G. Zhang, Z. Z. Zhang, Y. R. Sui and G. Wang, *ACS Appl. Mater. Interfaces*, 2016, **8**, 17334–17342.
5 S. Y. Chen, A. Walsh, X. G. Gong and S. H. Wei, *Adv. Mater.*, 2013, **25**, 1522–1539.
6 A. Walsh, S. Y. Chen, S. H. Wei and X. G. Gong, *Adv. Energy Mater.*, 2012, **2**, 400–409.
7 J. Kim, H. Hiroi, T. K. Todorov, O. Gunawan, M. Kuwahara, T. Gokmen, D. Nair, M. Hopstaken, B. Shin, Y. S. Lee, W. Wang, H. Sugimoto and D. B. Mitzi, *Adv. Mater.*, 2014, **26**, 7427–7431.
8 D. B. Mitzi, O. Gunawan, T. K. Todorov, K. Wang and S. Guha, *Sol. Energy Mater. Sol. Cells*, 2011, **95**, 1421–1436.
9 K. Ramasamy, M. A. Malik and P. O'Brien, *Chem. Commun.*, 2012, **48**, 5703–5714.
10 Q. Tian, Y. Cui, G. Wang and D. Pan, *RSC Adv.*, 2015, **5**, 4184–4190.
11 Z.-Y. Xiao, Y.-F. Li, B. Yao, Z.-H. Ding, R. Deng, H.-F. Zhao, L.-G. Zhang and Z.-Z. Zhang, *RSC Adv.*, 2015, **5**, 103451–103457.
12 W. Wang, M. T. Winkler, O. Gunawan, T. Gokmen, T. K. Todorov, Y. Zhu and D. B. Mitzi, *Adv. Energy Mater.*, 2014, **4**, 1301465.
13 S. Ahmed, K. B. Reuter, O. Gunawan, L. Guo, L. T. Romankiw and H. Deligianni, *Adv. Energy Mater.*, 2012, **2**, 253–259.
14 M. E. Erkan, V. Chawla and M. A. Scarpulla, *J. Appl. Phys.*, 2016, **119**, 194504.
15 G. Sozzi, S. D. Napoli, R. Menozzi, B. Bissig, S. Buecheler and A. N. Tiwari, *Sol. Energy Mater. Sol. Cells*, 2017, **165**, 94–102.
16 K. Herz, A. Eicke, F. Kessler, R. Wachter and M. Powalla, *Thin Solid Films*, 2003, **431**, 392–397.
17 B. A. Chambers, G. G. Andersson, J. S. Quinton, J. Jasieniak, B. I. MacDonald, M. Ionescu, A. Deslandes, J. S. Quinton, J. J. Jasieniak and G. G. Andersson, *Sol. Energy Mater. Sol. Cells*, 2014, **125**, 164–169.
18 R. Kotipalli, B. Vermang, J. Joel, R. Rajkumar, M. Edoff and D. Flandre, *AIP Adv.*, 2015, **5**, 107101.
19 J. Löckinger, S. Nishiwaki, T. P. Weiss, B. Bissig, Y. E. Romanyuk, S. Buecheler and A. N. Tiwari, *Sol. Energy Mater. Sol. Cells*, 2018, **174**, 397–404.
20 S. Gatz, T. Dullweber, V. Mertens, F. Einsele and R. Brendel, *Sol. Energy Mater. Sol. Cells*, 2012, **96**, 180–185.
21 W.-C. Wang, M. C. Tsai, J. Yang, C. Hsu and M.-J. Chen, *ACS Appl. Mater. Interfaces*, 2015, **7**, 10228–10237.
22 L. Q. Zhu, Q. Fang, X. J. Wang, J. P. Zhang, M. Liu, G. He and L. D. Zhang, *Appl. Surf. Sci.*, 2008, **254**, 5439–5444.
23 G. L. Lu, F. Zheng, J. Q. Wang and W. Z. Shen, *Prog. Photovoltaics*, 2017, **25**, 280–290.
24 P. Casper, R. Hünig, G. Gomard, O. Kiowski, C. Reitz, U. Lemmer, M. Powalla and M. Hetterich, *Phys. Status Solidi RRL*, 2016, **10**, 376–380.
25 W.-W. Hsu, J. Y. Chen, T.-H. Cheng, S. C. Lu, W.-S. Ho, Y.-Y. Chen, Y.-J. Chien and C. W. Liu, *Appl. Phys. Lett.*, 2012, **100**, 023508.
26 P. Poodt, A. Lankhorst, F. Roozeboom, K. Spee, D. Maas and A. Vermeer, *Adv. Mater.*, 2010, **22**, 3564–3567.
27 N. M. Terlinden, G. Dingemans, M. C. M. Van de Sanden and W. M. M. Kessels, *Appl. Phys. Lett.*, 2010, **96**, 112101.
28 L. Meng, B. Yao, Y. F. Li, Z. H. Ding, Z. Y. Xiao, K. S. Liu and G. Wang, *J. Alloys Compd.*, 2017, **710**, 403–408.
29 K. Wang, B. Shin, K. B. Reuter, T. Todorov, D. B. Mitzi and S. Guha, *Appl. Phys. Lett.*, 2011, **98**, 051912.
30 S. W. Shin, J. H. Han, Y. C. Park, G. L. Agawane, C. H. Jeong, J. H. Yun, A. V. Moholkar, J. Y. Lee and J. H. Kim, *J. Mater. Chem.*, 2012, **22**, 21727.
31 H.-J. Jeong, Y.-C. Kim, S. K. Lee, Y. Jeong, J.-W. Song, J.-H. Yun and J.-H. Jang, *ACS Appl. Mater. Interfaces*, 2017, **9**, 25404–25411.
32 S.-Y. Han, C. Q. Pan, D.-H. Kim and C.-H. Chang, *RSC Adv.*, 2015, **5**, 24712–24717.
33 L. Q. Zhu, Y. H. Liu, H. L. Zhang, H. Xiao and L. Q. Guo, *Appl. Surf. Sci.*, 2014, **288**, 430–434.
34 P. Menna, G. Di Francia and V. La Ferrara, *Sol. Energy Mater. Sol. Cells*, 1995, **37**, 13–24.
35 Y. T. Qu, G. Zoppi and N. S. Beattie, *Prog. Photovoltaics*, 2016, **24**, 836–845.
36 C. Van der Marel, M. Yildirim and H. R. Stapert, *J. Vac. Sci. Technol., A*, 2005, **23**, 1456.
37 V. Naumann, M. Otto, R. B. Wehrspohn, M. Werner and C. Hagendorf, *Energy Procedia*, 2012, **27**, 312–318.
38 Y.-W. Cheng, F.-L. Tang, H.-T. Xue, H.-X. Liu and B. Gao, *Appl. Surf. Sci.*, 2017, **394**, 58–62.